Latin American Journal of Solids and Structures
www.lajss.org

Uncertainty analysis of a flexible rotor supported by fluid film bearings

Abstract

This paper is dedicated to the analyses of the effect of uncertain parameters on the dynamic behavior of a flexible rotor containing two rigid discs and supported by two fluid film bearings. A stochastic method has been extensively used to model uncertain parameters, i.e., the so-called Monte Carlo simulation. However, in the present contribution, the inherent uncertainties of the bearings' parameters (i.e. the oil viscosity as a function of the oil temperature, and the radial clearance) are modeled by using a fuzzy dynamic analysis. This alternative methodology seems to be more appropriated when the stochastic process that models the uncertainties is unknown. The analysis procedure is confined to the time domain, being generated by the envelopes of the rotor orbits and the unbalance responses obtained from a run-down operating condition. The hydrodynamic supporting forces are determined by considering a nonlinear model, which is based on the solution of the dimensionless Reynolds' equation for cylindrical and short journal bearings. This numerical study illustrates the versatility and convenience of the mentioned fuzzy approach for uncertainty analysis. The results from the stochastic analysis are also presented for comparison purposes.

Keywords

Rotating machine; uncertainty analysis; fluid film bearings; fuzzy analysis.

Aldemir Ap Cavalini Jr.[a*]
Fabian Andres Lara-Molina[b]
Thiago de Paula Sales[c]
Edson Hideki Koroishi[d]
Valder Steffen Jr.[e]

[a,c,e]LMEst – Structural Mechanics Laboratory, Federal University of Uberlândia, School of Mechanical Engineering, Uberlândia, MG, Brazil

[b,d]Federal Technological University of Paraná, Campus Cornélio Procópio, Cornélio Procópio, PR, Brazil

Corresponding author:
*aacjunior@mecanica.ufu.br

http://dx.doi.org/10.1590/1679-78251582

Received 14.09.2014
Accepted 10.03.2015
Available online 02.05.2015

1 INTRODUCTION

The computational simulation of rotating machines is an indispensable resource for engineers. It allows a comprehensive understanding about the dynamic behavior of the system, considering the amount of variables involved in the problem (Meggiolaro, 1996). Thereby, a mathematical model capable of representing satisfactorily the dynamic behavior of a rotating machine is obtained by

taking into account various subsystems, as follows: first, the subsystems that are defined by their geometry, as the shaft, drives and couplings; later, the gyroscopic effect; finally, the subsystems that are frequency and/or state dependent, such as the hydrodynamic bearings. The bearings are one of the most critical subsystems of the rotor system, influencing significantly the performance, life, and reliability of the machine. According to Vance et al. (2010), many problems in rotating systems can be attributed to the design and application of the bearings. Thus, understanding the physical phenomena that involve the bearings is essential to improve the dynamic performance of the system.

The hydrodynamic bearings represent an important component of rotating machinery due to their large use in the industry (Riul, 1988). In this case, the load is supported by a thin film of lubricant that separates the shaft from the bearing (i.e., there is no direct contact between metal parts). Thus, this subsystem can theoretically offer infinite life, considering that the rotor operates under safe dynamic conditions and with clean lubricant (Vance et al., 2010). It is worth mentioning that due to the oil film, the damping effect on hydrodynamic bearings is more pronounced than in rolling bearings, which is beneficial in machines that go through critical speeds during startup and stop down procedures. In this context, the analysis of uncertainties either in the geometry (e.g., radial clearance, due to the machining processes or damage) or in the operating conditions (e.g., oil temperature) that affect the performance of the hydrodynamic bearings is an important design issue.

Uncertainty analysis of flexible rotors has been studied by applying stochastic approaches based on the stochastic finite element method (Ghanem and Spanos, 1991). Didier et al. (2011) quantified the uncertainties effects in the response of flexible rotors based on the Polynomial Chaos theory. Koroishi et al. (2012) represented the uncertainties in the rotor parameters by using Gaussian homogeneous stochastic fields discretized by Karhunen-Loève expansion; the dynamic response of the system with random parameters was characterized through Hypercube Latin sampling and Monte Carlo simulation. Lara-Molina et al. (2014) used the fuzzy stochastic finite element method to quantify the effects of high order random parameters on the response of a rotating machine.

In agreement with the fuzzy approach, the present work proposes the application of a straightforward approach to simulate the dynamic response of a flexible rotor with random parameters by performing a fuzzy dynamic analysis. For this purpose, the fuzzy uncertain parameters are mapped onto the model with the aid of the so-called α-level optimization (Möller and Beer, 2004). Additionally, the Differential Evolution algorithm is used to solve the optimization problem in the fuzzy analysis (Price et al., 2005). For comparison purposes, the Monte Carlo simulation combined with Latin Hypercube sampling is used to generate the envelope of responses of the stochastic rotor system. The choice of this stochastic solver is justified by the fact that Monte Carlo simulation has been successfully used as a reference stochastic solver to evaluate the variability of the dynamic responses (Sampaio and Cataldo, 2010). Two uncertainty scenarios are analyzed: (a) the first case is dedicated to the influence of uncertainties on the oil viscosity of both bearings of the rotating system (i.e., oil temperature); (b) the second case is associated to the introduction of uncertainties in the radial clearance of the bearings. As the uncertainties are analyzed only in the bearings' parameters, the Monte Carlo simulation is directly applied to the deterministic finite element model of the rotor (Koroishi et al., 2012).

2 ROTOR MODELING

Equation (1) presents the matrix differential equation that model the dynamic behavior of a flexible rotor supported by fluid film bearings (Lalanne and Ferraris, 1998).

$$M\,\ddot{q} + \left[D + \Omega\, D_g\right]\dot{q} + \left[K + \dot{\Omega}\, K_{st}\right]q = W + F_u + F_h \tag{1}$$

where M is the mass matrix, D is the damping matrix (i.e., proportional damping), D_g represents the gyroscopic effect, K is the stiffness matrix, and K_{st} is the stiffness matrix resulting from the transient motion. All these matrices are related to the rotating parts of the system, such as couplings, discs, and the shaft. The vector q contains the generalized displacements, and Ω is the shaft rotation speed. W stands for the weight of the rotating parts, F_u represents the unbalance forces, and F_h is the vector of the shaft supporting forces produced by the hydrodynamic bearings. The shaft is modeled by using Timoshenko's beam elements (finite element model) with two nodes and four degrees of freedom per node (i.e., two displacements and two rotations).

3 HYDRODYNAMIC BEARING MODEL REVIEW

In this work, the hydrodynamic supporting forces are determined by following the approach proposed by Capone (1986). This nonlinear model is based on the solution of the dimensionless Reynolds' equation for cylindrical and short journal bearings (Figure 1), as expressed by Equation (2).

$$\left(\frac{R}{L_h}\right)^2 \frac{\partial}{\partial \overline{y}}\left(\overline{h}_h^3 \frac{\partial \overline{p}_h}{\partial \overline{y}}\right) = \frac{\partial \overline{h}_h}{\partial \theta} + 2\dot{\overline{h}}_h \tag{2}$$

where $\overline{p}_h = \overline{p}_h\left(\theta, \overline{y}\right)$ is the pressure distribution on the bearing (Equation (3); μ_h is the oil viscosity), $\overline{y}$ is the longitudinal coordinate of the shaft center O_E (on the bearing location), θ is the cylindrical coordinate, R is the shaft radius, L_h is the length of the bearing, and $\overline{h}_h$ is the oil film thickness ($\overline{h}_h = 1 - \overline{x}\cos\theta - \overline{z}\sin\theta$); $\overline{x} = x/C$ and $\overline{z} = z/C$ are the coordinates of O_E along the X and Z directions, respectively; $\dot{\overline{x}} = \dot{x}/\left(\Omega C\right)$ and $\dot{\overline{z}} = \dot{z}/\left(\Omega C\right)$, where C is the radial clearance of the bearing. The overbar denotes dimensionless quantities. The bearing surface is assumed to be stationary.

$$\overline{p}_h = \frac{p_h}{6\mu_h \Omega\left(R/L_h\right)^2} \tag{3}$$

The simplifications applied to Reynolds' equation allow its direct integration, leading to the analytical form for the pressure field (Equation (4)); $\overline{p}_h(\theta, \pm 0.5) = 0$ are defined as the boundary conditions.

$$\overline{p}_h\left(\theta, \overline{y}\right) = \frac{1}{8}\left(\frac{L_h}{R}\right)^2 \left[\frac{\left(\overline{x} - 2\dot{\overline{z}}\right)\sin\theta - \left(\overline{z} + 2\dot{\overline{x}}\right)\cos\theta}{\overline{h}_h^3}\right]\left(4\overline{y}^2 - 1\right) \tag{4}$$

The hydrodynamic forces F_h are determined by the integration of Equation (4) over the bearing supporting area.

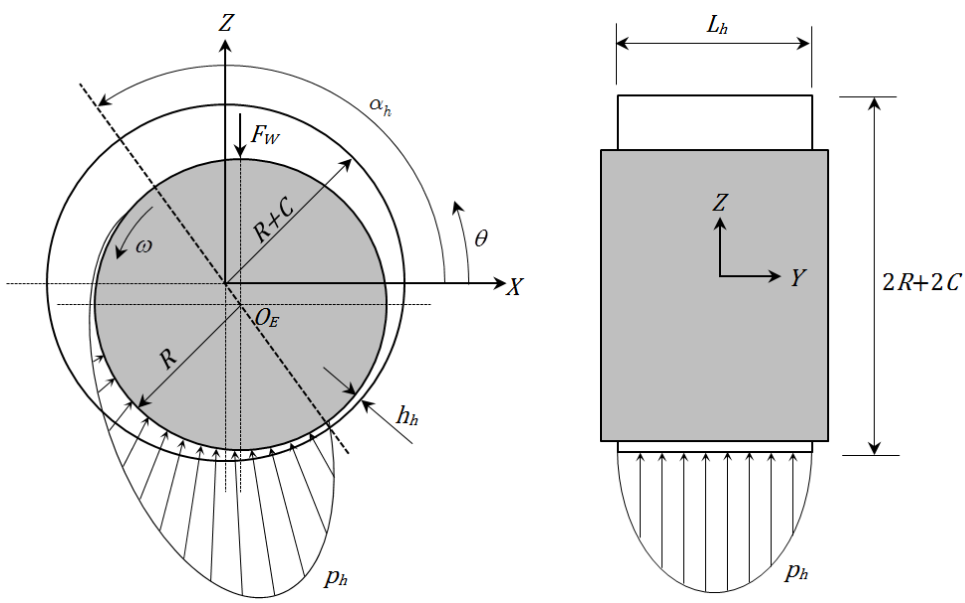
$$F_h = -\frac{6\mu\omega R^3}{L_h}\int_{-1/2}^{1/2}\int_{\alpha_h}^{\alpha_h+\pi} \overline{p}_h\left(\theta,\overline{y}\right)\begin{Bmatrix}\cos\theta\\ \sin\theta\end{Bmatrix}\mathrm{d}\theta\,\mathrm{d}\overline{y} \tag{5}$$

where α_h is the attitude angle defined by the Equation (6).

$$\alpha_h = \tan^{-1}\left(\frac{\overline{z}+2\dot{\overline{x}}}{\overline{x}-2\dot{\overline{z}}}\right) - \frac{\pi}{2}\,\mathrm{sign}\left(\frac{\overline{z}+2\dot{\overline{x}}}{\overline{x}-2\dot{\overline{z}}}\right) - \frac{\pi}{2}\,\mathrm{sign}\left(\overline{z}+2\dot{\overline{x}}\right) \tag{6}$$

To find the analytical expression for the hydrodynamic forces, the solution of the integral G_h, Equation (7), is used to solve the Equation (5) as shown below.

$$G_h = \int_{\alpha_h}^{\alpha_h+\pi}\frac{1}{1-\overline{x}\cos\theta-\overline{z}\sin\theta}\mathrm{d}\theta = \frac{2}{\left(1-\overline{x}^2-\overline{z}^2\right)^{1/2}}\left[\frac{\pi}{2}+\tan^{-1}\left(\frac{\overline{z}\cos\alpha_h-\overline{x}\sin\alpha_h}{\left(1-\overline{x}^2-\overline{z}^2\right)^{1/2}}\right)\right] \tag{7}$$



(a) *XZ*-plane. (b) *YZ*-plane.

Figure 1: Cylindrical hydrodynamic bearing.

Therefore, the hydrodynamic force vector F_h is given by:

$$F_h = -\mu\Omega\frac{R\,L_h^3}{4C^2}\frac{\left[\left(\overline{z}+2\dot{\overline{x}}\right)^2+\left(\overline{x}-2\dot{\overline{z}}\right)^2\right]^{1/2}}{1-\overline{x}^2-\overline{z}^2}\begin{Bmatrix}3\overline{x}V_h - G_h\sin\alpha_h - 2S_h\cos\alpha_h\\ 3\overline{z}V_h + G_h\cos\alpha_h - 2S_h\sin\alpha_h\end{Bmatrix} \tag{8}$$

where V_h and S_h are defined as:

$$V_h = \frac{2 + \left(\overline{z}\cos\alpha_h - \overline{x}\sin\alpha_h\right)G_h}{1 - \overline{x}^2 - \overline{z}^2} \tag{9}$$

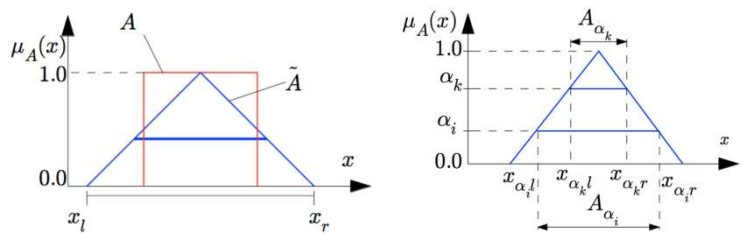
$$S_h = \frac{\overline{x}\cos\alpha_h + \overline{z}\sin\alpha_h}{1 - \left(\overline{x}\cos\alpha_h + \overline{z}\sin\alpha_h\right)^{1/2}} \tag{10}$$

4 FUZZY ANALYSIS

According to Lara-Molina et al. (2015), the random parameters of rotating machines can be modeled by using fuzzy theory as an alternative approach to the stochastic methods. By using the fuzzy theory, it is possible to describe incomplete and inaccurate information. The theory of fuzzy sets was initially formulated by Zadeh (1965) to characterize vague aspects of information. Thereafter, it was developed a different approach for fuzzy sets that can be compared with the theory of possibilities to deal with the uncertainty of information (Zadeh, 1978). Both theories are connected, so that the uncertainties are modeled by means of the theory of fuzzy sets for the cases in which the stochastic process that describes the random variables is unknown (Moens and Hanss, 2011; Waltz and Hanss, 2013). The basic concepts of the fuzzy variables are revisited next.

4.1 Fuzzy variables

Let X_F be an universal classical set of objects whose generic elements are denoted by x. The subset $A(A \in X_F)$ is defined by the classical membership function $\mu_A : X_F \rightarrow \{0, 1\}$, shown in Figure 2. Furthermore, a fuzzy set $\tilde{A}$ is defined by means of the membership function $\mu_A : X_F \rightarrow [0, 1]$, being $[0, 1]$ a continuous interval. The membership function indicates the degree of compatibility between the element x and the fuzzy set $\tilde{A}$. The closer is the value of $\mu_A(x)$ to 1, the more x belongs to $\tilde{A}$.



(a) Fuzzy set. (b) The α - levels.

Figure 2: Fuzzy set and α - level representation.

Thus, the fuzzy set is completely defined by:

$$\tilde{A} = \left\{\left(x, \mu_A(x)\right) \middle| x \in X_F\right\} \tag{11}$$

where $0 \leq \mu_A \leq 1$.

For computational purposes, the fuzzy set $\tilde{A}$ can be represented by means of subsets that are denominated α- levels. These subsets, which correspond to real and continuous intervals, are defined by $A_{\alpha k}$ (Figure 2), thus:

$$A_{\alpha k} = \left\{ x \in X_F, \mu_A(\mathrm{x}) \geq \alpha_k \right\} \tag{12}$$

The α- level subsets of $\tilde{A}$ have the property:

$$A_{\alpha k} \subseteq A_{\alpha i} \forall \alpha_i, \alpha_k \in \left[0, 1\right] \tag{13}$$

with $\alpha_i \leq \alpha_k$. If the fuzzy set is convex for the one-dimensional case, each α- level subset $A_{\alpha k}$ corresponds to the interval $[x_{\alpha k l}, x_{\alpha k r}]$, shown in Equation (14).

$$\begin{aligned} x_{\alpha k l} &= \min\left[x \in X_F \left| \mu_A(x) \geq \alpha_k \right. \right] \\ x_{\alpha k r} &= \max\left[x \in X_F \left| \mu_A(x) \geq \alpha_k \right. \right] \end{aligned} \tag{14}$$

4.2 Dynamic models with fuzzy parameters

In this work, the dynamic model describes the behavior of the rotor by means of a set of differential equations. The relationship between the inputs $\mathbf{x}$ and outputs $\mathbf{z}$ of a specific dynamic model M_f is characterized by f, which represents the set of differential equations of the model in Equation (15).

$$M_f : \mathbf{z}(\tau) = f(\mathbf{x}) \tag{15}$$

Therefore, the function f maps the inputs $\mathbf{x}$ onto the outputs $\mathbf{z}(\tau)$. Thus, $\mathbf{x} \rightarrow \mathbf{z}(\tau)$, where τ is the independent variable of the dynamic response that may represent time, frequency or spatial coordinates. Considering the inputs of the model as fuzzy variables $\tilde{\mathbf{x}}$ or fuzzy functions $\tilde{\mathbf{x}}(\tau)$, the dynamic response of the system corresponds to the resulting fuzzy functions $\tilde{\mathbf{z}}(\tau)$. These fuzzy functions result from the mapping, thus $\tilde{\mathbf{x}} \rightarrow \tilde{\mathbf{z}}(\tau)$.

4.3 Fuzzy dynamic analysis

The fuzzy dynamic analysis is an appropriate method to map a fuzzy input vector $\tilde{\mathbf{x}}$ onto the output $\tilde{\mathbf{z}}(\tau)$ of a numerical model by using the deterministic model given by Equation (15). In structural analysis, the combination of uncertainties modeled as fuzzy variables with the deterministic model based on the finite element method is denominated fuzzy finite element method. The fuzzy dynamic analysis includes two stages, as shown in Figure 3.

In the first stage, for computational purposes, the input vector that corresponds to the fuzzy parameter is discretized by means of the α- level representation, presented in the Equation (12) and Figure 2. Thus, each element of the fuzzy parameters vector $\tilde{\mathbf{x}} = (\tilde{x}_1,...,\tilde{x}_n)$ is considered as an interval $X_{i\alpha k} = \left[x_{i\alpha k l}, x_{i\alpha k r} \right]$, where $\alpha_k \in \left[0,1\right]$. Consequently, the sub-space $\mathbf{X}_{\alpha k}$ is defined so that $\mathbf{X}_{\alpha k} = (\mathbf{X}_{1\alpha k},...,\mathbf{X}_{n\alpha k})$, where $\mathbf{X}_{\alpha k} \in \mathbb{R}^n$.

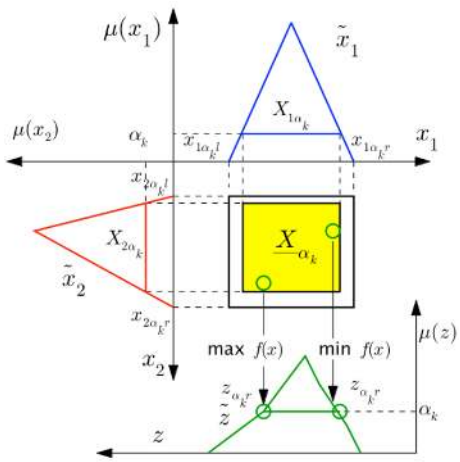


Figure 3: The α - level optimization.

The second stage is related to solving an optimization problem. This optimization problem consists in finding the maximum or minimum value of the output, at each value of τ, for the mapping model $M_f : \mathbf{z}(\tau) = f(\mathbf{x})$. Thus:

$$\begin{aligned} z_{\alpha kl} &= \min_{\mathbf{x}\in\mathbf{X}_{\alpha k}} f(\mathbf{x}) \\ z_{\alpha kr} &= \max_{\mathbf{x}\in\mathbf{X}_{\alpha k}} f(\mathbf{x}) \end{aligned} \tag{16}$$

where $z_{\alpha kl}$ and $z_{\alpha kr}$ correspond to the upper and lower bounds of the interval $z_{\alpha k} = \left[z_{\alpha kl},\, z_{\alpha kr}\right]$ in the α - level α_k. The set of discretized intervals $[z_{\alpha kl},\, z_{\alpha kr}]$ for $\alpha_k \in (0,1]$ composes the whole fuzzy resulting variable $\tilde{z}$.

The fuzzy analysis of a transient time-domain system demands the solution of a large number of optimization problems regarding all α - level of interest for each considered time step. In this paper, each upper and lower bounds of the system analysis at a given time instant is obtained from the Differential Evolution optimization algorithm (Price et al., 2005). The output value of the transient analysis at the evaluated time-step constitutes the objective function. The inputs to this function are the uncertain parameters described previously as fuzzy or fuzzy random variables.

5 NUMERICAL RESULTS

The proposed uncertainty analysis was applied to a horizontal rotating machine modeled by using 16 Timoshenko beam elements, which is shown in Figure 4. The finite element model is composed by a flexible steel shaft with 780 mm length and 12 mm diameter ($E = 2.07\text{x}10^{11}$ Pa, $\rho = 7800$ kg/m^3, and $\upsilon = 0.3$), two rigid discs D_1 (node #8) and D_2 (node #11), both of steel with 100 mm diameter and 20 mm thickness ($\rho = 7800$ kg/m^3), and two cylindrical hydrodynamic bearings (B_1 and B_2, located at the nodes #4 and #14, respectively), each one with 25 mm diameter, 10 mm length, and radial clearance $C = 50\,\mu$m (i.e., the deterministic radial clearance). The hypothesis of short sleeve bearing is justified from the bearings dimensions. In this application, the oil viscosity is equal to 0.04 Pa.s (i.e., the deterministic oil viscosity, ISO VG 68 at 45°C). The rotating parts take into account a proportional damping ($D_p = \beta K$) with the coefficient $\beta = 2\text{x}10^{-4}$.

The effects of the coupling between the electric motor and the shaft are disregarded. Displacement responses are collected at the bearings and discs locations along the horizontal and vertical directions (X and Z , respectively). An unbalance of 100 g.mm at 0^{o} was applied to each disc of the rotor. Figure 5a illustrates the displacement obtained in the horizontal direction of the bearing B_1 in a linear run-down condition (3200 to 100 rev/min in 30 sec). Figure 5b shows the hydrodynamic force developed on the vertical direction of the bearing B_1 considering the same operational condition. It is possible to observe that the first critical speed of the rotating machine is, approximately, 1500 rev/min. The solution of the equations was obtained by using the trapezoidal rule integration scheme, which was coupled with the Newton-Raphson iterative method for nonlinear equations, as described in Appendix A.

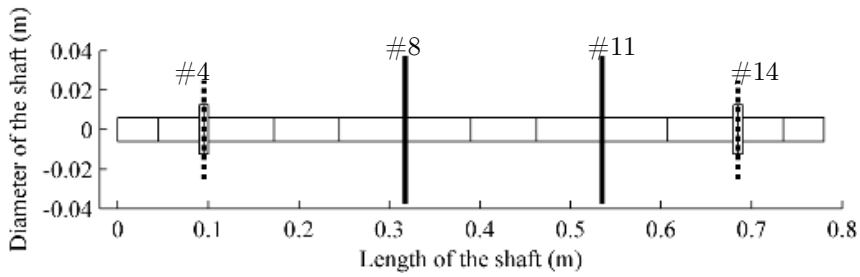
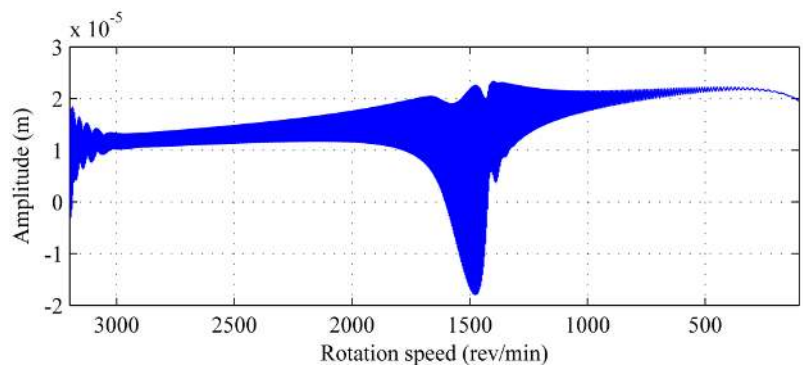
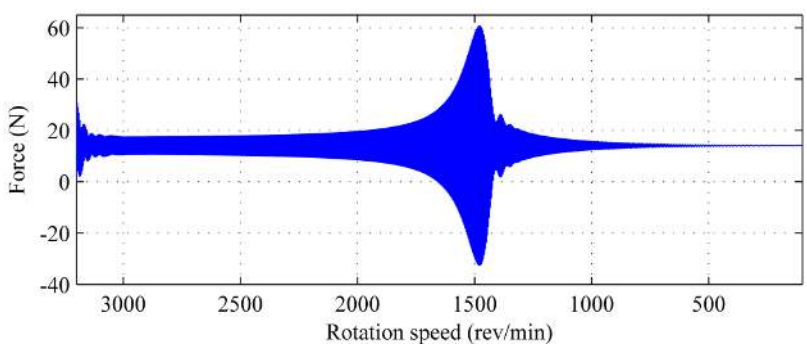


Figure 4: FE model of the rotor (····· bearing; —— disc).



(a) Horizontal displacement obtained at the bearing B_1.



(b) Vertical force developed at the bearing B_1.

Figure 5: Rotor performing a linear run-down condition.

As mentioned, two uncertainty scenarios are considered in the present work. The first scenario is dedicated to analyze the influence of uncertainties only in the oil temperature of both bearings, by changing the oil viscosity μ_h. The second one takes into account only uncertainties in the radial clearances of B_1 and B_2. In both scenarios, the measured orbits of the rotor operating at 1000 rev/min are analyzed.

Concerning the application of the fuzzy analysis, the uncertain parameters were modeled by using fuzzy triangular numbers. Thus,

$$\tilde{a} = a\left(1 - \frac{p_s}{100} \;/\; 1 \;/\; 1 + \frac{p_s}{100}\right) \tag{17}$$

where a represents the nominal value of the parameter and p_s stands for the maximum percentage of amplitude in $\alpha_k = 0$. In this work $p_s = 5$, corresponding to the two uncertainty scenarios (i.e., 5 % of variation around the nominal value).

In order to solve the optimization problem associated to the described fuzzy analysis, the following parameters were used for the Differential Evolution algorithm: 10 individuals in the initial population, 100 generations, crossover probability rate of 0.5, perturbation rate of 0.8, and the strategy for the mutation mechanism was DE/rand/1/bin (Lobato et al., 2010). The instantaneous radius of the orbit obtained on the bearing B_1 (deterministic radius R_{B_1}) was considered as being the objective function of the minimization and maximization problems (see Equation (16)) associated to the fuzzy analysis.

$$R_{B_1} = \left(X^2 + Z^2\right)^{1/2} \tag{18}$$

Considering the Monte Carlo simulation, the first step was to determine the number of sampling n_s to be used in the stochastic modeling. For this purpose, a sensitivity analysis has been performed based on the instantaneous radius R_{B_1} obtained from Equation (18). The convergence analysis was performed according to the following expression:

$$C_{n_s j} = \frac{\left\| \bar{R}_{B_1 j} - R_{B_1} \right\|}{\left\| R_{B_1} \right\|} \tag{19}$$

where $\bar{R}_{B_1}$ is the instantaneous radius of the orbit determined from different values of n_s (i.e., the stochastic radius) and $j = 1,2,...,n_s$. It is worth mentioning that both uncertainty scenarios were taken into account simultaneously for this evaluation (i.e., 5 % of variation in the oil viscosity and in the radial clearance). Additionally, the uncertain random parameters were modeled by using Gaussian random variables. Figure 6 show the convergence evaluation of the n_s value used in the stochastic analysis. Note that the convergence was achieved for $n_s = 200$.

Figure 7 shows the orbits obtained in two measurement planes, located at bearing B_1 and disc D_1, considering both fuzzy and stochastic analyses, for the first uncertainty scenario (i.e., uncertainty on the oil viscosity). Note that the disc responses (Figures 7c and 7d) were affected by

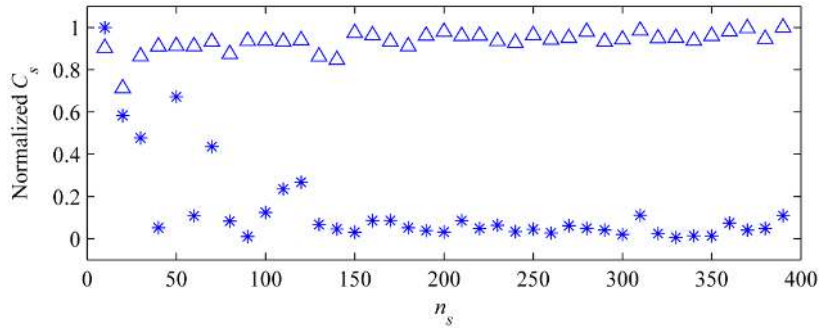
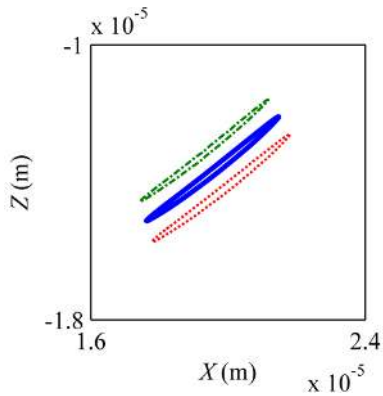
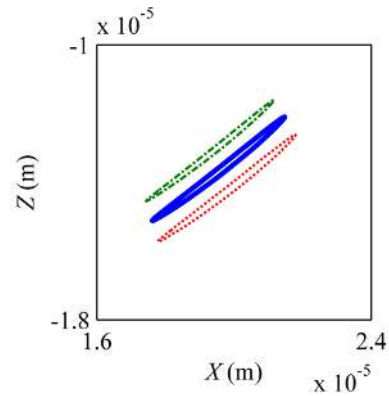


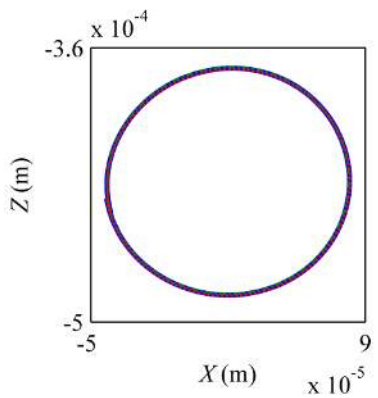
Figure 6: Convergence evaluation of the number of sampling (* lower limit; △ upper limit).



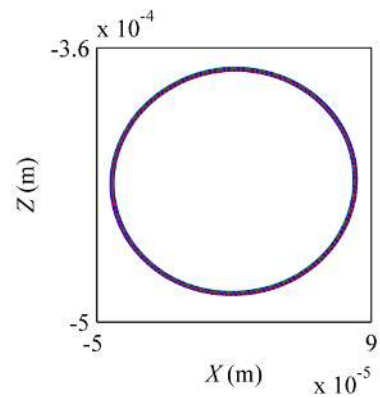
(a) Fuzzy analysis: bearing B_1.



(b) Stochastic analysis: bearing B_1.



(c) Fuzzy analysis: disc D_1.

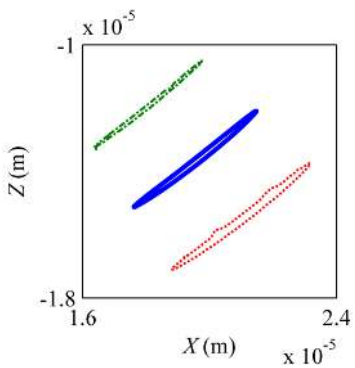


(d) Stochastic analysis: disc D_1.

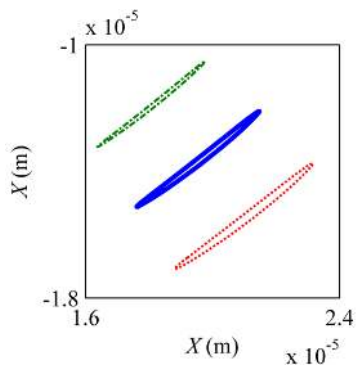
Figure 7: Envelope of the orbits considering the uncertainty on the oil viscosity (— nominal; ···· lower limit / $\alpha = 0$; -·-·- upper limit / $\alpha = 0$).

minor variations, while the uncertainty parameter changed significantly the orbits at the bearings (Figures 7a and 7b). The center of the orbits moved downward according to the decreasing viscosity. This is an expected result, since the hydrodynamic force F_h (Equation (8)) is proportional to the oil viscosity (the force decreases with the decreasing viscosity). Additionally, it can be seen that both uncertainty analyses provided similar results (by comparing Figures 7a with 7b and 7c with 7d). The results obtained from the other two measurement planes were similar.

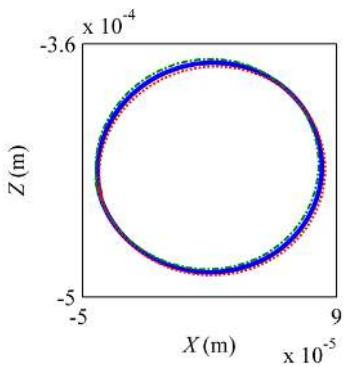
Figure 8 shows the orbits obtained in the two measurement planes depicted in Figure 7, considering both fuzzy and stochastic analyses, but now for the second uncertainty scenario (i.e., uncertainty on the radial clearance). As observed in Figure 7, the responses of the disc (Figures 8c and 8d) were affected by minor variations as compared with the orbits at the bearings (Figures 8a and 8b). In this case, the center of the orbits moved downward according to the increasing radial clearance. Equation (8) shows that F_h is proportional to the inverse of the square of the radial clearances (the force decreases with the increasing radial clearance). Both uncertainty analyses provided similar results. However, some irregularities can be observed in the responses obtained at the bearings, for the case in which the fuzzy approach was applied (see Figure 8a). One attributes such abnormal behavior to the optimization process that needs to be carried out for the determination of each displacement point of the orbits. Additionally, it can be seen that uncertainties in the radial clearances (Figure 8) were able to modify significantly the rotor responses. Note that smaller changes are observed in the results obtained from the uncertainties introduced in the oil viscosity (Figure 7). Simultaneous uncertainty has also been considered for both oil viscosity and radial clearance. In this case, the results were similar to those shown in Figure 8. It is worth mentioning that all shown results are specific for rotating machines supported by fluid film bearings. Koroishi et al. (2012) show that for a rotating machine supported by ball bearings the orbits remains concentric if uncertainties are considered for the stiffness and damping coefficients of the bearings.



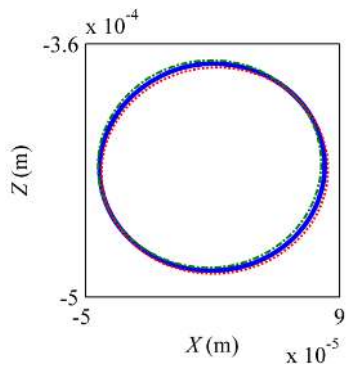
(a) Fuzzy analysis: bearing B_1.



(b) Stochastic analysis: bearing B_1.



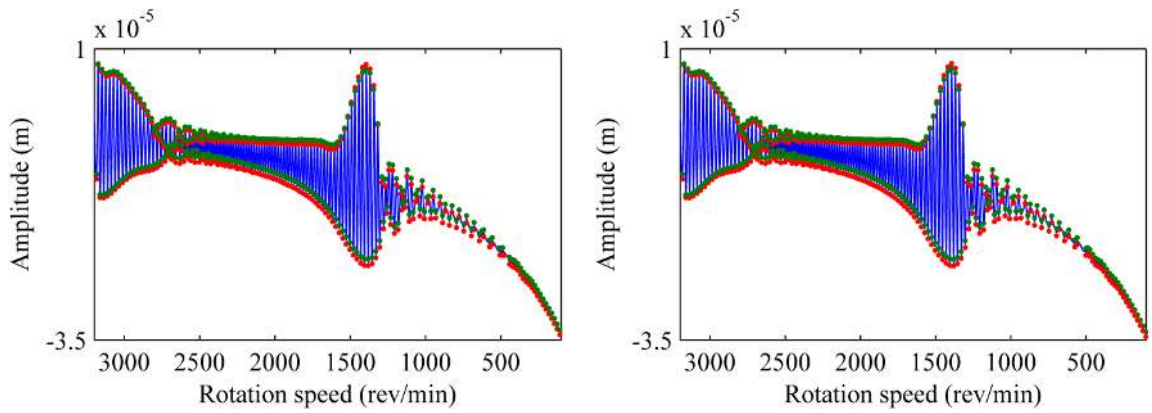
(c) Fuzzy analysis: disc D_1.



(d) Stochastic analysis: disc D_1.

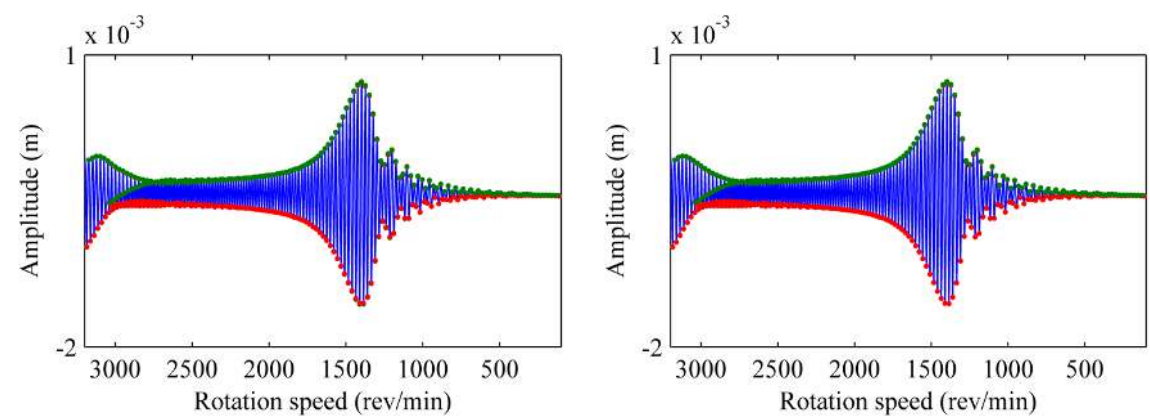
Figure 8: Envelope of the orbits considering the uncertainty on the radial clearance (— nominal; ···· lower limit / $\alpha = 0$; -·-·- upper limit / $\alpha = 0$).

Figure 9 show the responses obtained along the Z direction on the same two measurement planes considered earlier, for the rotor operating under a linear run-down condition (3200 to 100 rev/min in 30 sec). The first uncertainty scenario is evaluated for both fuzzy and stochastic analyses. The instantaneous radius of the orbit obtained at the bearing B_1 was considered as being the objective function for the minimization and maximization problems associated to the fuzzy analysis (see Equation (18)). Considering the Monte Carlo simulation, it has been considered $n_s = 200$, according to the convergence evaluation shown in Figure 6. Note that the disc responses (Figures 9c and 9d) are affected by minor variations. Additionally, it can be seen that both uncertainty analyses again provide similar results (by comparing Figures 9a with 9b, and 9c with 9d). The results obtained from the other two measurement planes are similar, and thus they were not included in this contribution.



(a) Fuzzy analysis: bearing B_1.

(b) Stochastic analysis: bearing B_1.



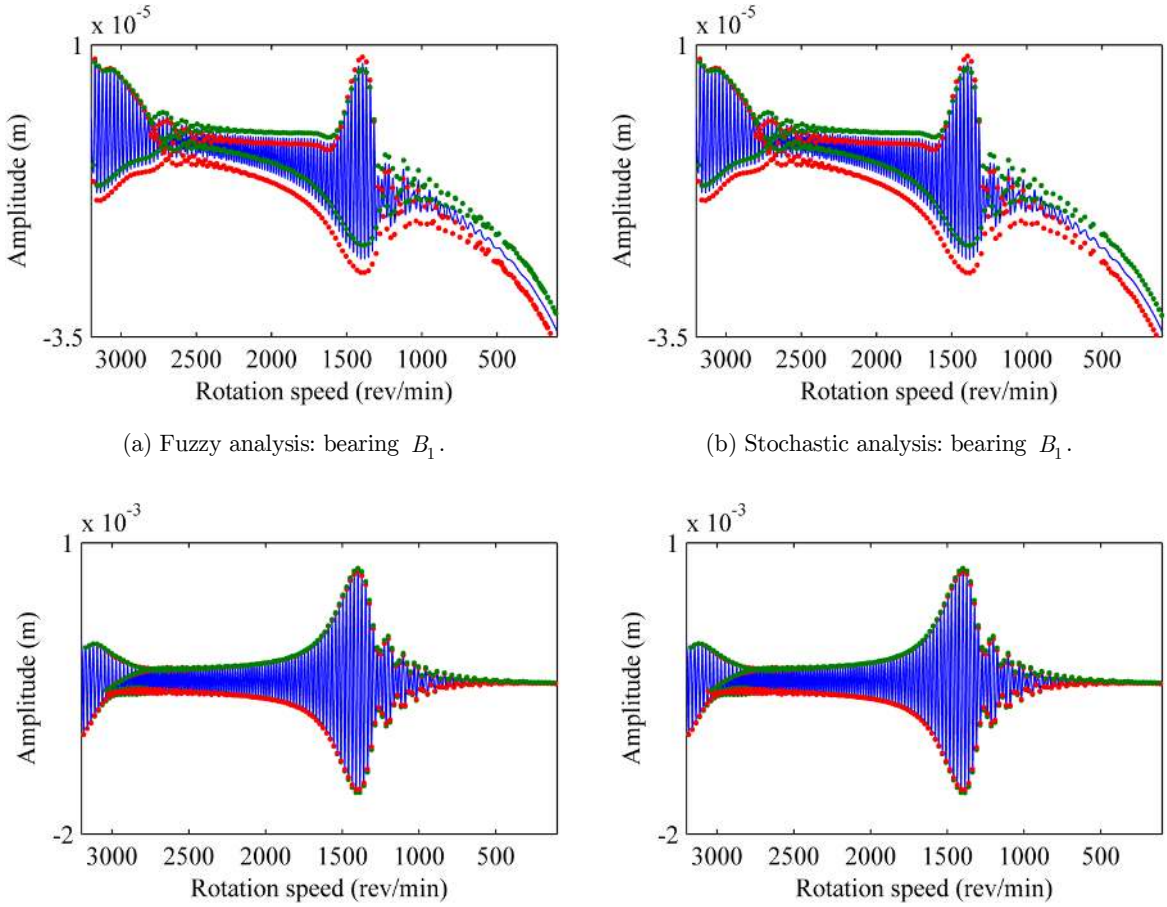
(c) Fuzzy analysis: disc D_1.

(d) Stochastic analysis: disc D_1.

Figure 9: Envelope of the run-down responses considering the uncertainty on the oil viscosity (— nominal; ···· lower limit / $\alpha = 0$; ···· upper limit / $\alpha = 0$).

Figure 10 also shows the responses obtained along the Z direction for the same two measurement planes, located at bearing B_1 and disc D_1, with the rotor operating under a linear run-down

condition (3200 to 100 rev/min in 30 sec). However, in this case the second uncertainty scenario (i.e., uncertainty on the radial clearance) is evaluated for both fuzzy and stochastic analyses. As observed in Figure 9, the responses of the disc (Figures 10c and 10d) were affected by minor variations as compared with the responses of the bearings (Figures 10a and 10b).



(a) Fuzzy analysis: bearing B_1.

(b) Stochastic analysis: bearing B_1.

(c) Fuzzy analysis: disc D_1.

(d) Stochastic analysis: disc D_1.

Figure 10: Envelope of the run-down responses considering uncertainty in the radial clearance (— nominal; ···· lower limit / $\alpha = 0$; ···· upper limit / $\alpha = 0$).

Again, both uncertainty analyses provided similar results. From Figures 10a and 10b, it can be seen that the lower limit (i.e., the red points) is associated with the largest radial clearance. Remember that the center of the orbits moved downward according to the increasing radial clearance (see Figure 8). Clearly, the green points are associated with the smallest radial clearances. A similar analysis can be done considering the Figure 9. Additionally, note that the uncertainties in the radial clearances (Figure 10) were able to modify significantly the run-down rotor responses. Smaller changes are observed in the results obtained from the uncertainties introduced in the oil viscosity (Figure 9).

6 CONCLUSIONS

In this paper two uncertainty approaches were used to evaluate the dynamic responses of a flexible rotor supported by oil film bearings, namely fuzzy and stochastic analyses. Two uncertainty scenarios were analyzed: uncertainties in the oil viscosity and uncertainties in the radial clearance (all applied simultaneously to both bearings). The numerical applications show that both uncertainty approaches led to similar results. However, the fuzzy analysis seems to be more adequate when the stochastic process that models the uncertain parameters of the bearings is not well defined. Finally, the proposed strategy demonstrates the relevance of introducing uncertainties in the design variables from the design perspective of rotating machinery. Moreover, the stochastic approach requires the estimation of the probability density function of the uncertain parameters. Further studies will encompass an experimental verification.

Acknowledgements

The authors are thankful to the Brazilian Research Agencies FAPEMIG and CNPq (INCT-EIE) and also to CAPES for the financial support provided to this research effort.

References

Capone, G., (1986). Orbital motions of rigid symmetric rotor supported on Journal Bearings. La Meccanica Italiana 199: 37-46.

Didier, J., Faverjon, B., Sinou, J.J., (2011). Analyzing the dynamic response of a rotor system under uncertain parameters polynomial chaos expansion. Journal of Vibration and Control 18: 712-732.

Ghanem, R.G., Spanos, P.D., (1991). Stochastic finite elements – A Spectral Approach. Spring Verlag New York, Inc.

Koroishi, E.H., Cavalini Jr., A.A., de Lima, A.M.G., Steffen Jr., V., (2012). Stochastic modeling of flexible rotors. Journal of the Brazilian Society of Mechanical Sciences and Engineering 34: 597-603.

Lalanne, M., Ferraris, G., (1998). Rotordynamics prediction in engineering. John Wiley and Sons.

Lara-Molina, F.A., Koroishi, E.H., Steffen Jr., V., (2014). Fuzzy stochastic dynamic analysis of flexible rotors. Proceedings of the 2nd International Symposium on Uncertainty Quantification and Stochastic Modeling 1: 25-36.

Lara-Molina, F.A., Koroishi, E.H., Steffen Jr., V., (2015). Uncertainty analysis of flexible rotors considering fuzzy parameters and fuzzy-random parameters. Latin American Journal of Solids and Structures, in press.

Lobato, F.S., Steffen Jr., V., Silva Neto, A.J., (2010). Solution of inverse radiative transfer problems in two-layer participating media with differential evolution. Inverse Problems in Science & Engineering 18: 183-195.

Meggiolaro, M.A., (1996). Modelagem de mancais hidrodinâmicos na simulação de sistemas rotativos. MSc Thesis, Pontifícia Universidade Católica do Rio de Janeiro, Brazil.

Moens, D., Hanss, M., (2011). Non-probabilistic finite element analysis for parametric uncertainty treatment in

applied mechanics: recent advances. Finite Elements in Analysis and Design 47: 4-16.

Möller, B., Beer, M., (2004). Fuzzy randomness, uncertainty in civil engineering and computational mechanics. Springer Verlag.

Price, K.V., Storn, R.M., Lampinen, J.A., (2005). Differential evolution a practical approach to global optimization. Springer Verlag.

Riul, J.A., (1988). Estudo teórico e experimental de mancais hidrodinâmicos cilíndricos. MSc Thesis, Universidade Federal de Uberlândia, Brazil.

Sampaio, R., Cataldo, E., (2010). Comparing two strategies to model uncertainties in structural dynamics. Shock and Vibration 14: 171-186.

Vance, J., Zeidan, F., Murphy, B., (2010). Machinery vibration and rotordynamics. John Wiley & Sons, Inc.

Waltz, N.P., Hanss, M., (2013). Fuzzy arithmetical analysis of multibody systems with uncertainties. The archive of mechanical engineering 1: 109-125.

Zadeh, L., (1965). Fuzzy Sets. Information and Control 8: 338-353.

Zadeh, L., (1978). Fuzzy Sets as Basis for a Theory of Possibility. Fuzzy Sets and Systems 1: 3-28.

APPENDIX A

Numerical integration of the equations of motion.

Section 3 shows that the hydrodynamic bearing force is nonlinear in the bearing degrees of freedom $\overline{x}$ and $\overline{z}$ (see Equations (6) to (10)). Thus, direct numerical integration of Equation (1) is not possible, as it consists of a nonlinear, second-order differential system of equations. Hence, to obtain the time responses, the Newton-Raphson method is considered in conjunction with the Newmark-type, trapezoidal rule integration algorithm. One considers the solution to be known for time t, and, from the dynamic equilibrium equations, one wants to compute the solution for time $t+\Delta t$. First, one writes:

$$M\,\ddot{q}_{t+\Delta t} + \left[D + \Omega_{t+\Delta t}\,D_g\right]\dot{q}_{t+\Delta t} + \left[K + \dot{\Omega}_{t+\Delta t}\,K_{st}\right]q_{t+\Delta t} = W + \left(F_u\right)_{t+\Delta t} + \left(F_h\right)_{t+\Delta t} \tag{A1}$$

where the right-subscript indicates the discrete-time evaluation of the quantity.

One writes,

$$\left(F_h\right)_{t+\Delta t} = \left(F_h\right)_{t+\Delta t}\left(q_{t+\Delta t}\ ,\ \dot{q}_{t+\Delta t}\right) \tag{A2}$$

which render the system nonlinear, as stated above.

It is assumed an approximate solution set for Equation (A1), as shown by Equation (A3).

$$\left(q_{t+\Delta t}^{(n+1)}\ ,\ \dot{q}_{t+\Delta t}^{(n+1)}\ ,\ \ddot{q}_{t+\Delta t}^{(n+1)}\right) \tag{A3}$$

where n is the Newton-Raphson iteration-related index.

Firstly, Equation (A1) is written in the form of a residual (Equation (A4)) by moving R.H.S. quantities to its L.H.S..

$$R\left(q_{t+\Delta t}^{(n+1)}\ ,\ \dot{q}_{t+\Delta t}^{(n+1)}\ ,\ \ddot{q}_{t+\Delta t}^{(n+1)}\right) = 0 \tag{A4}$$

Then, this result is expanded in the form of a Taylor series, as follows:

$$R\left(q_{t+\Delta t}^{(n+1)}\ ,\ \dot{q}_{t+\Delta t}^{(n+1)}\ ,\ \ddot{q}_{t+\Delta t}^{(n+1)}\right) = R\left(q_{t+\Delta t}^{(n)}\ ,\ \dot{q}_{t+\Delta t}^{(n)}\ ,\ \ddot{q}_{t+\Delta t}^{(n)}\right) + \left.\frac{\partial R}{\partial q}\right|_{t+\Delta t}^{(n)} \Delta q_{t+\Delta t}^{(n)} + \left.\frac{\partial R}{\partial \dot{q}}\right|_{t+\Delta t}^{(n)} \Delta \dot{q}_{t+\Delta t}^{(k)} + \left.\frac{\partial R}{\partial \ddot{q}}\right|_{t+\Delta t}^{(n)} \Delta \ddot{q}_{t+\Delta t}^{(n)} + H.O.T. \tag{A5}$$

in which $H.O.T.$ stands for Higher Order Terms. Additionally,

$$\Delta \,\mathrm{var}_{t+\Delta t}^{(n)} = \mathrm{var}_{t+\Delta t}^{(n+1)} - \mathrm{var}_{t+\Delta t}^{(n)} \tag{A6}$$

where $\mathrm{var} = \left\{q, \dot{q}, \ddot{q}\right\}$.

Disregarding the Higher Order Terms, and considering the trapezoidal rule integration algorithm relations:

$$\begin{aligned} \Delta q_{t+\Delta t}^{(n)} &= \left(\tfrac{1}{2}\Delta t\right)^2 \Delta \ddot{q}_{t+\Delta t}^{(n)} \\ \Delta \dot{q}_{t+\Delta t}^{(n)} &= \tfrac{1}{2}\Delta t\ \Delta \ddot{q}_{t+\Delta t}^{(n)} \end{aligned} \tag{A7}$$

the following iterative equation is established:

$$T_{t+\Delta t}^{(n)} \Delta \ddot{q}_{t+\Delta t}^{(n)} = -R\left(q_{t+\Delta t}^{(n)}\ ,\ \dot{q}_{t+\Delta t}^{(n)}\ ,\ \ddot{q}_{t+\Delta t}^{(n)}\right) \tag{A8}$$

where

$$\begin{aligned} T_{t+\Delta t}^{(n)} &= \left(\tfrac{1}{2}\Delta t\right)^2 \left.\frac{\partial R}{\partial q}\right|_{t+\Delta t}^{(n)} + \left(\tfrac{1}{2}\Delta t\right) \left.\frac{\partial R}{\partial \dot{q}}\right|_{t+\Delta t}^{(n)} + \left.\frac{\partial R}{\partial \ddot{q}}\right|_{t+\Delta t}^{(n)} \\ &= \left(\tfrac{1}{2}\Delta t\right)^2 \left\{K + \dot{\Omega}_{t+\Delta t}\, K_{st} - \left.\frac{\partial F_h}{\partial q}\right|_{t+\Delta t}^{(n)}\right\} + \left(\tfrac{1}{2}\Delta t\right)\left\{D + \Omega_{t+\Delta t}\, D_g - \left.\frac{\partial F_h}{\partial \dot{q}}\right|_{t+\Delta t}^{(n)}\right\} + M \end{aligned} \tag{A9}$$

The solution $\ddot{q}_{t+\Delta t}^{(n+1)}$ is obtained from first solving Equation (A8), and then using Equation (A6).

Other unknown variables are calculated from Equation (A7). The procedure is repeated until convergence criteria are met, such as obtained by Equation (A10) and/or Equation (A11). Results presented along the paper were obtained by considering $\varepsilon_{NR} = 10^{-6}$.

$$\left\| R\left(q_{t+\Delta t}^{(n+1)}\ ,\ \dot{q}_{t+\Delta t}^{(n+1)}\ ,\ \ddot{q}_{t+\Delta t}^{(n+1)}\right)\right\| < \varepsilon_{NR} \tag{A10}$$

$$\left\| \Delta \ddot{q}_{t+\Delta t}^{(n)} \right\| < \varepsilon_{NR} \tag{A11}$$

The difficult part in evaluating the coefficients matrix (Equation (A9)) lies in calculating the derivatives of the hydrodynamic bearing force vector F_h with respect to the degree of freedom vector and its time-derivative. These expressions correspond to the linear stiffness and damping coefficients of a

hydrodynamic bearing. Such terms have been previously obtained by Meggiolaro (1996), and are written as follows:

$$\begin{Bmatrix} k_{XX} \\ k_{ZX} \end{Bmatrix} = -\frac{1}{C}\frac{\partial F_h}{\partial \overline{x}} = \frac{\mu_h \Omega R}{4}\left(\frac{L}{C}\right)^3 \left[\left(\frac{v}{mn} + \frac{2\overline{x}n}{m^2}\right)H + \frac{n}{m}\frac{\partial H}{\partial \overline{x}}\right]$$

$$\begin{Bmatrix} k_{XZ} \\ k_{ZZ} \end{Bmatrix} = -\frac{1}{C}\frac{\partial F_h}{\partial \overline{z}} = \frac{\mu_h \Omega R}{4}\left(\frac{L}{C}\right)^3 \left[\left(\frac{u}{mn} + \frac{2\overline{z}n}{m^2}\right)H + \frac{n}{m}\frac{\partial H}{\partial \overline{z}}\right]$$

$$\begin{Bmatrix} d_{XX} \\ d_{ZX} \end{Bmatrix} = -\frac{1}{C\Omega}\frac{\partial F_h}{\partial \dot{\overline{x}}} = \frac{\mu_h R}{4}\left(\frac{L}{C}\right)^3 \left[\frac{2u}{mn}H + \frac{n}{m}\frac{\partial H}{\partial \dot{\overline{x}}}\right] \tag{A12}$$

$$\begin{Bmatrix} d_{XX} \\ d_{ZX} \end{Bmatrix} = -\frac{1}{C\Omega}\frac{\partial F_h}{\partial \dot{\overline{z}}} = \mu_h \frac{\mu_h R}{4}\left(\frac{L}{C}\right)^3 \left[-\frac{2v}{mn}H + \frac{n}{m}\frac{\partial H}{\partial \dot{\overline{z}}}\right]$$

where $u = \overline{z} + 2\dot{\overline{x}}$, $v = \overline{x} - 2\dot{\overline{z}}$, $n = \left(u^2 + v^2\right)^{1/2}$, and $m = 1 - \overline{x}^2 - \overline{z}^2$. The vector H is defined by Equation (A13).

$$H = \begin{Bmatrix} 3\overline{x}V_h - G_h \operatorname{sen}\alpha_h - 2S_h \cos\alpha_h \\ 3\overline{z}V_h + G_h \cos\alpha_h - 2S_h \operatorname{sen}\alpha_h \end{Bmatrix} \tag{A13}$$

For the proper use of Equation (A12) in evaluating Equation (A9), the following derivatives are necessary:

$$\frac{\partial H}{\partial \overline{x}} = \begin{Bmatrix} 3V_h + 3\overline{x}\dfrac{\partial V_h}{\partial \overline{x}} - G_h\dfrac{\partial \alpha_h}{\partial \overline{x}}\cos\alpha_h - \dfrac{\partial G_h}{\partial \overline{x}}\sin\alpha_h + 2S_h\dfrac{\partial \alpha_h}{\partial \overline{x}}\sin\alpha_h - 2\dfrac{\partial S_h}{\partial \overline{x}}\cos\alpha_h \\ 3\overline{z}\dfrac{\partial V_h}{\partial \overline{x}} - G_h\dfrac{\partial \alpha_h}{\partial \overline{x}}\sin\alpha_h + \dfrac{\partial G_h}{\partial \overline{x}}\cos\alpha_h - 2S_h\dfrac{\partial \alpha_h}{\partial \overline{x}}\cos\alpha_h - 2\dfrac{\partial S_h}{\partial \overline{x}}\sin\alpha_h \end{Bmatrix}$$

$$\frac{\partial H}{\partial \overline{z}} = \begin{Bmatrix} 3\overline{x}\dfrac{\partial V_h}{\partial \overline{z}} - G_h\dfrac{\partial \alpha_h}{\partial \overline{z}}\cos\alpha_h - \dfrac{\partial G_h}{\partial \overline{z}}\sin\alpha_h + 2S_h\dfrac{\partial \alpha_h}{\partial \overline{z}}\sin\alpha_h - 2\dfrac{\partial S_h}{\partial \overline{z}}\cos\alpha_h \\ 3V_h + 3\overline{z}\dfrac{\partial V_h}{\partial \overline{z}} - G_h\dfrac{\partial \alpha_h}{\partial \overline{z}}\sin\alpha_h + \dfrac{\partial G_h}{\partial \overline{z}}\cos\alpha_h - 2S_h\dfrac{\partial \alpha_h}{\partial \overline{z}}\cos\alpha_h - 2\dfrac{\partial S_h}{\partial \overline{z}}\sin\alpha_h \end{Bmatrix}$$

$$\frac{\partial H}{\partial \dot{\overline{x}}} = \begin{Bmatrix} 3\overline{x}\dfrac{\partial V_h}{\partial \dot{\overline{x}}} - G_h\dfrac{\partial \alpha_h}{\partial \dot{\overline{x}}}\cos\alpha_h - \dfrac{\partial G_h}{\partial \dot{\overline{x}}}\sin\alpha_h + 2S_h\dfrac{\partial \alpha_h}{\partial \dot{\overline{x}}}\sin\alpha_h - 2\dfrac{\partial S_h}{\partial \dot{\overline{x}}}\cos\alpha_h \\ 3\overline{z}\dfrac{\partial V_h}{\partial \dot{\overline{x}}} - G_h\dfrac{\partial \alpha_h}{\partial \dot{\overline{x}}}\sin\alpha_h + \dfrac{\partial G_h}{\partial \dot{\overline{x}}}\cos\alpha_h - 2S_h\dfrac{\partial \alpha_h}{\partial \dot{\overline{x}}}\cos\alpha_h - 2\dfrac{\partial S_h}{\partial \dot{\overline{x}}}\sin\alpha_h \end{Bmatrix} \tag{A14}$$

$$\frac{\partial H}{\partial \dot{\overline{z}}} = \begin{Bmatrix} 3\overline{x}\dfrac{\partial V_h}{\partial \dot{\overline{z}}} - G_h\dfrac{\partial \alpha_h}{\partial \dot{\overline{z}}}\cos\alpha_h - \dfrac{\partial G_h}{\partial \dot{\overline{z}}}\sin\alpha_h + 2S_h\dfrac{\partial \alpha_h}{\partial \dot{\overline{z}}}\sin\alpha_h - 2\dfrac{\partial S_h}{\partial \dot{\overline{z}}}\cos\alpha_h \\ 3\overline{z}\dfrac{\partial V_h}{\partial \dot{\overline{z}}} - G_h\dfrac{\partial \alpha_h}{\partial \dot{\overline{z}}}\sin\alpha_h + \dfrac{\partial G_h}{\partial \dot{\overline{z}}}\cos\alpha_h - 2S_h\dfrac{\partial \alpha_h}{\partial \dot{\overline{z}}}\cos\alpha_h - 2\dfrac{\partial S_h}{\partial \dot{\overline{z}}}\sin\alpha_h \end{Bmatrix}$$

$$\frac{\partial \alpha_h}{\partial \overline{x}} = -\frac{u}{u^2 + v^2} \qquad \frac{\partial \alpha_h}{\partial \overline{z}} = \frac{v}{u^2 + v^2} \qquad \frac{\partial \alpha_h}{\partial \dot{\overline{x}}} = \frac{2v}{u^2 + v^2} \qquad \frac{\partial \alpha_h}{\partial \dot{\overline{z}}} = \frac{2u}{u^2 + v^2} \tag{A15}$$

$$\frac{\partial V_h}{\partial \overline{x}} = \frac{\left[p\frac{\partial G_h}{\partial \overline{x}} - \left(q\frac{\partial \alpha_h}{\partial \overline{x}} + \sin\alpha_h\right)G_h\right]m + 2\overline{x}\left(2 + pG_h\right)}{m^2}$$

$$\frac{\partial V_h}{\partial \overline{z}} = \frac{\left[p\frac{\partial G_h}{\partial \overline{z}} - \left(q\frac{\partial \alpha_h}{\partial \overline{z}} - \cos\alpha_h\right)G_h\right]m + 2\overline{z}\left(2 + pG_h\right)}{m^2} \tag{A16}$$

$$\frac{\partial V_h}{\partial \dot{\overline{x}}} = \frac{\left[p\frac{\partial G_h}{\partial \dot{\overline{x}}} - q\frac{\partial \alpha_h}{\partial \dot{\overline{x}}}G_h\right]}{m} \qquad \frac{\partial V_h}{\partial \dot{\overline{z}}} = \frac{\left[p\frac{\partial G_h}{\partial \dot{\overline{z}}} - q\frac{\partial \alpha_h}{\partial \dot{\overline{z}}}G_h\right]}{m}$$

$$\frac{\partial S_h}{\partial \overline{x}} = \left(p\frac{\partial \alpha_h}{\partial \overline{x}} + \cos\alpha_h\right)\frac{1+q^2}{\left(1-q^2\right)^2} \qquad \frac{\partial S_h}{\partial \overline{z}} = \left(p\frac{\partial \alpha_h}{\partial \overline{z}} + \sin\alpha_h\right)\frac{1+q^2}{\left(1-q^2\right)^2}$$

$$\frac{\partial S_h}{\partial \dot{\overline{x}}} = p\frac{\partial \alpha_h}{\partial \dot{\overline{x}}}\frac{1+q^2}{\left(1-q^2\right)^2} \qquad \frac{\partial S_h}{\partial \dot{\overline{z}}} = p\frac{\partial \alpha_h}{\partial \dot{\overline{z}}}\frac{1+q^2}{\left(1-q^2\right)^2} \tag{A17}$$

$$\frac{\partial G_h}{\partial \overline{x}} = \frac{\overline{x}}{m^{3/2}}\left[\pi + 2\tan^{-1}\left(\frac{p}{m^{1/2}}\right)\right] + 2\frac{\left(\frac{p\overline{x}}{m} - q\frac{\partial \alpha_h}{\partial \overline{x}} - \sin\alpha_h\right)}{m + p^2}$$

$$\frac{\partial G_h}{\partial \overline{z}} = \frac{\overline{z}}{m^{3/2}}\left[\pi + 2\tan^{-1}\left(\frac{p}{m^{1/2}}\right)\right] + 2\frac{\left(\frac{p\overline{z}}{m} - q\frac{\partial \alpha_h}{\partial \overline{z}} + \cos\alpha_h\right)}{m + p^2} \tag{A18}$$

$$\frac{\partial G_h}{\partial \dot{\overline{x}}} = -2\frac{\left(q\frac{\partial \alpha_h}{\partial \dot{\overline{x}}}\right)}{m + p^2} \qquad \frac{\partial G_h}{\partial \dot{\overline{z}}} = -2\frac{\left(q\frac{\partial \alpha_h}{\partial \dot{\overline{z}}}\right)}{m + p^2}$$

where $p = \overline{z}\cos\alpha_h - \overline{x}\sin\alpha_h$ and $q = \overline{x}\cos\alpha_h + \overline{z}\sin\alpha_h$.